

AN EVOLVING ENTROPY FLOOR IN THE INTRACLUSTER GAS?

WENJUAN FANG¹ AND ZOLTÁN HAIMAN²

Draft version February 2, 2008

ABSTRACT

Non-gravitational processes, such as feedback from galaxies and their active nuclei, are believed to have injected excess entropy into the intracluster gas, and therefore to have modified the density profiles in galaxy clusters during their formation. Here we study a simple model for this so-called preheating scenario, and ask (i) whether it can simultaneously explain both global X-ray scaling relations and number counts of galaxy clusters, and (ii) whether the amount of entropy required evolves with redshift. We adopt a baseline entropy profile that fits recent hydrodynamic simulations, modify the hydrostatic equilibrium condition for the gas by including $\approx 20\%$ non-thermal pressure support, and add an entropy floor K_0 that is allowed to vary with redshift. We find that the observed luminosity–temperature ($L - T$) relations of low-redshift ($\langle z \rangle = 0.05$) HIFLUGCS clusters and high-redshift ($\langle z \rangle = 0.80$) WARPS clusters are best simultaneously reproduced with an evolving entropy floor of $K_0(z) = 341(1+z)^{-0.83}h^{-1/3}\text{keV cm}^2$. If we restrict our analysis to the subset of bright ($kT \gtrsim 3\text{ keV}$) clusters, we find that the evolving entropy floor can mimic a self-similar evolution in the $L - T$ scaling relation. This degeneracy with self-similar evolution is, however, broken when ($0.5 \lesssim kT \lesssim 3\text{ keV}$) clusters are also included. The $\sim 60\%$ entropy increase we find from $z = 0.8$ to $z = 0.05$ is roughly consistent with that expected if the heating is provided by the evolving global quasar population. Using the cosmological parameters from the *WMAP* 3-year data with $\sigma_8 = 0.76$, our best-fit model underpredicts the number counts of the X-ray galaxy clusters compared to those derived from the 158deg^2 ROSAT PSPC survey. Treating σ_8 as a free parameter, we find a best-fit value of $\sigma_8 = 0.80 \pm 0.02$, in good agreement with the results from a recent combined analysis of the Lyman- α forest, 3D weak lensing and *WMAP* 3-year data. For the flux-limited cluster catalogs, we include an intrinsic scatter in log-luminosity at both fixed temperature ($\sigma_{\ln L|T} \approx 0.3$) and at fixed mass ($\sigma_{\ln L|M} \approx 0.6$), but we find this does not have a big effect on our results.

Subject headings: cosmology: theory; galaxies: clusters: general – intergalactic medium – X-rays: galaxies: clusters

1. INTRODUCTION

Galaxy clusters, the most massive bound objects in the universe, provide several methods to constrain cosmological models, for example through their abundance (e.g., Evrard 1989; Henry & Arnaud 1991; White, Efstathiou & Frenk 1993; Eke, Cole & Frenk 1996; Viana & Liddle 1999; Mantz et al. 2007), or their spatial distribution (Schuecker et al. 2001; Refregier, Valtchanov, & Pierre 2002; Hu & Haiman 2003; Blake & Glazebrook 2003; Seo & Eisenstein 2003; Linder 2003), or both (Schuecker et al. 2003). In large future surveys, with tens of thousands of clusters, percent-level statistical constraints are expected to be available on dark energy parameters (Haiman, Mohr & Holder 2001), including constraints on the evolution of its equation of state parameter $w_a \equiv -dw/da$ (Weller, Battye, & Kneissl 2002; Weller & Battye 2003; Wang et al. 2004).

In order to fully realize the cosmological potential of large cluster samples, it is important to understand the cluster mass-observable relations accurately, at least statistically. It is very unlikely that the structure of clusters will be understood from ab-initio calculations to the level of precision required for the theoretical uncertainties not to dominate over the exquisite statistical errors (e.g.

Levine, Schultz, & White 2002). However, in principle, when multiple observables depend on the same mass, the mass-observable relation can be accurately determined from the data itself, simultaneously with cosmological parameters. Several works have proposed and quantified the constraints from such ‘self-calibration’ (Majumdar & Mohr 2004; Wang et al. 2004; Lima & Hu 2005), using parameterized phenomenological relations for the mass-observable relations (for example, power-law scalings, or arbitrary evolution in pre-specified redshifts bins). It has been argued recently (Younger et al. 2006) that even if cluster structure is not precisely predictable, parameterized physical models can further improve on such phenomenological self-calibration, especially when multiple observables (such as X-ray flux and Sunyaev-Zel’dovich [SZ] decrement) can be predicted from the same physical model (Younger et al. 2006). In light of this potential, it is important to fit physically motivated cluster models to as many cluster observables as possible; one then hopes that future observations of larger cluster samples will require further fine-tuning of these models, and, at the same time, deliver useful cosmological constraints (Ostriker, Bode & Babul 2005; Younger et al. 2006).

The gravitational potential of clusters is dominated by dark matter, whose behavior is determined by gravity alone, and is therefore robustly predictable. The dark matter profiles of galaxy clusters, apart from the innermost regions, are indeed well understood from three-

¹ Department of Physics, Columbia University, New York, NY 10027; wjfang@phys.columbia.edu

² Department of Astronomy, Columbia University, New York, NY 10027; zoltan@astro.columbia.edu

dimensional numerical simulations (Navarro, Frenk & White 1997; Moore et al. 1998), and are nearly self-similar, as expected. The physics of gas, on the other hand, involves complicated non-gravitational processes such as radiative cooling and star formation, galaxy evolution, and various forms of feedback. If these processes were unimportant, the intracluster gas would trace the self-similar dark matter profile, and its global properties should obey simple scaling relations (Kaiser 1986). Specifically, its X-ray luminosity L , if dominated by thermal Bremsstrahlung, as for clusters with temperature $T > 2$ keV, should scale as $L \propto T^2$. This relation is indeed obeyed by clusters in hydrodynamic simulations without non-gravitational processes (Evrard, Metzler, & Navarro 1996; Bryan & Norman 1998). However, the observed $L - T$ scaling relation is significantly steeper than the self-similar prediction, closer to $L \propto T^3$ (Markevich 1998; Arnaud & Evrard 1999). This demonstrates that the effect of non-gravitational processes on the intracluster gas is not negligible, even for “bulk” observables.

A long-standing proposal for the dominant such non-gravitational effect is that the intracluster gas is heated by some energy input (from star formation, supernovae explosion, galactic winds and/or active galactic nuclei [AGN]), raising the gas to a higher adiabat before the clusters collapse. Many authors have investigated the effect of such a preheating, and have shown that simply imposing a minimum “entropy floor” for the intracluster gas naturally breaks the self-similarity, and steepens the $L - T$ relation as required by the data (Kaiser 1991; Evrard & Henry 1991; Cavaliere, Menci, & Tozzi 1997; Tozzi & Norman 2001; Babul et al. 2002; Voit et al. 2002). The pre-heating idea is further supported by the discovery of excess entropy in the inner regions of low-temperature clusters, which suggests the existence of a universal entropy floor (Ponman, Cannon & Navarro 1999; Lloyd-Davies, Ponman, & Cannon 2000), and by several other independent lines of evidence (for a brief summary and a list of references, see, e.g., Bialek, Evrard & Mohr 2001).

A simple model of pre-heating consists of shifting the entropy profile by an overall additive constant, representing the cumulative effect of non-gravitational processes, assumed to be roughly uniform throughout the gas (e.g. Voit et al. 2002). Recent work has tested this simple model, by comparing its predictions with hydrodynamical simulations (Younger & Bryan 2007, hereafter YB07). The model reproduces the simulation results very well, but comparisons with observations show that although it can predict the global X-ray scaling relations, the model can not reproduce the observed entropy profiles (Ponman, Sanderson, & Finoguenov 2003; Pratt & Arnaud 2005; Pratt, Arnaud, & Pointecouteau 2006) in detail. This requires the model to be further developed, but as far as the global properties are concerned, it appears to be successful, and it is therefore useful to understand the average properties of the intracluster gas.

In this paper, we adopt this simple preheating model, and focus on comparisons with both the observed $L - T$ scaling relations in the redshift range $0 \lesssim z \lesssim 1$, and the observed cumulative number counts of the X-ray clusters. A previous study (Bialek, Evrard & Mohr 2001) calculated the impact of preheating on the X-ray scaling relations, using a sample of 12 simulated clusters, and

found a good fit to the data on local clusters (but has not explicitly compared the expected evolution to observations, and has not made simultaneous predictions for the number counts). Our work is also somewhat similar to a more recent study by Ostriker, Bode & Babul (2005), who present a more detailed physical model for the intracluster gas, and show that it can reproduce local X-ray scaling relations (this paper also did not study evolution).

Our goal here is to clarify (i) whether the model can simultaneously explain both the scaling relations *and* number counts of galaxy clusters, and (ii) whether the amount of entropy required evolves with redshift. In comparing our predictions to the $L - T$ scaling relations and the number counts, we also study the effects of scatter in the $L - T$ and $L - M$ relations, and the corresponding selection biases that arise in flux limited survey (Nord et al. 2007). Our first goal is motivated by our earlier study (Younger et al. 2006), in which we found that a similar preheating model, with the entropy adjusted to reproduce observed X-ray and SZ scaling relations, tends to overpredict the number counts of bright clusters, even with a relatively low normalization ($\sigma_8 = 0.7$) of the power spectrum. A similar discrepancy was found by Ostriker, Bode & Babul (2005, although they used a higher normalization, $\sigma_8 = 0.84$, and suggested that agreement can be recovered by lowering this value).

The rest of this paper is organized as the follows. In § 2, we describe in detail the formalism to implement the preheating model. In § 3, we compare the predicted $L - T$ scaling relations to observations, and find the best-fit entropy level K_0 at two different redshifts. In § 4, we further test the model by comparing predictions for the number counts with observations. In § 5, we then study the effect of intrinsic scatters and the corresponding selection effects in flux-limited cluster surveys. In § 6, we discuss our results, and in § 7, we offer our conclusions.

2. MODIFIED ENTROPY MODEL OF PREHEATING

We adopt the terminology from the literature, and refer to the quantity

$$K = \frac{P}{\rho_g^\gamma} \quad (1)$$

as “entropy”. Here P and ρ_g are the pressure and density of the gas, and γ is the adiabatic index. For an ideal gas, K is related to the formal thermodynamic entropy per particle s by $s - s_0 \propto \ln K$, with s_0 a constant. In this paper, the baseline entropy profile to be modified is adopted from YB07³, which is a fit to that of the clusters in AMR simulations (Voit, Kay & Bryan 2005) without non-gravitational processes. The profile is self-similar when expressed as a function of the gas fraction f_g , and

³ To examine the sensitivity of our conclusions below to the choice of this baseline profile, we also tried adopting the entropy profile of gas that traces the DM distribution in an NFW halo. We have verified that our main conclusion below, that the entropy floor increases with cosmic time, still holds in this case. In particular, following the procedure in Younger et al. (2006), but assuming $f_g = 0.9$ and 20% non-thermal pressure support, we find K_0 increases from 363^{+65}_{-61} at $z = 0.8$ to $507^{+17}_{-17} h^{-1/3}$ keV cm² at $z = 0.05$ (these numbers include intrinsic scatter, and are to be compared with the values obtained in our fiducial model in § 5.1).

normalized by K_{vir} ,

$$\frac{K(f_g)}{K_{\text{vir}}} = 0.18 + 0.2f_g + 1.5f_g^2. \quad (2)$$

Here $f_g(< r) = M_g(< r)/(f_b M_{\text{vir}})$ is the gas mass inside radius r , normalized by the cosmic mass fraction of baryons ($f_b = \Omega_b/\Omega_m$) times the total virial mass of the cluster M_{vir} . We further define $T_{\text{vir}} = GM_{\text{vir}}\mu m_p/(2r_{\text{vir}})$, which is the temperature of the corresponding isothermal sphere (Voit et al. 2002). (Throughout this paper, we absorb k_B into T , so temperature is in units of energy.) The mean molecular weight $\mu = 0.59$ is adopted for the intracluster gas, appropriate for a fully ionized H-He plasma with helium mass fraction $Y_{\text{He}} = 0.25$; m_p is the mass of proton, and r_{vir} is the virial radius. K_{vir} is then calculated by $K_{\text{vir}} = T_{\text{vir}}/(f_b \rho_{\text{vir}})^{\gamma-1}/(\mu m_p)$, where ρ_{vir} is the mean density of the cluster within the virial radius (relates M_{vir} to r_{vir} by $M_{\text{vir}} = \frac{4\pi}{3}\rho_{\text{vir}} r_{\text{vir}}^3$, see below for its calculation).

The effect of preheating is then realized by adding a constant K_0 to $K(f_g)$,

$$K^{\text{ph}}(f_g) = K(f_g) + K_0, \quad (3)$$

where the value of K_0 can be determined once the amount of energy injected into the cosmic gas, and the density of the gas at the time of the injection, is specified. Convective stability requires the specific entropy K to be a monotonically increasing function of radius (Voit et al. 2002), and hence of f_g . The above prescription of preheating may change f_g as a function of r , but it does not change the order of the gas shells. The entropy profile, together with the hydrostatic equilibrium and gas mass conservation equations,

$$\frac{dP}{dr} = -\eta \rho_g \frac{GM_{\text{tot}}(< r)}{r^2} \quad (4)$$

$$\frac{dM_g(< r)}{dr} = 4\pi r^2 \rho_g \quad (5)$$

can be used to solve for the pressure and density distribution of the intracluster gas. Combined with the equation of state for ideal gases, the temperature profile of the gas also follows from the solutions. In equation (4), $M_{\text{tot}}(< r) = M_{\text{DM}}(< r) + M_g(< r)$. The dark matter profile $M_{\text{DM}}(< r)$ is known, and is given below. Including η allows deviations from strict hydrostatic equilibrium. Here we adopt $\eta = 0.8$, the value YB07 find in their simulations, suggesting that the remaining support for the gas is provided by turbulent motions.

The boundary condition for $M_g(< r)$ is naturally chosen to be zero at the origin (to avoid numerical difficulties, in practice we give M_g a small value at some small finite radius). The pressure at the same position is found by giving it a trial value and integrating equations (4-5) until the pressure at r_{vir} matches the expected momentum flux of infalling gas,

$$P(r_{\text{vir}}) = \frac{1}{3} f_b \rho_{\text{NFW}}(r_{\text{vir}}) v_{\text{ff}}^2. \quad (6)$$

Here we assume the accreting gas is cold (Voit et al. 2003), and that it falls freely from the turnaround radius (r_{ta}) and is shocked at the virial radius. We assume $r_{\text{ta}} = 2r_{\text{vir}}$, so that the free-fall velocity v_{ff} from r_{ta} to

r_{vir} is given by $v_{\text{ff}}^2 = GM_{\text{vir}}/r_{\text{vir}} (= 2T_{\text{vir}}/\mu m_p)$. The postshock gas density is $f_b \rho_{\text{NFW}}$ (see below for the calculation of ρ_{NFW}). Under extreme conditions, the free-fall kinetic energy is totally transformed into thermal energy, and the post-shock gas has a pressure as given above; this value agrees with that adopted in YB07, matching their simulation results. (Besides the difference in identifying clusters, our boundary pressure has a numerical factor of $\frac{2}{3}$ compared to theirs of 0.7.) These two boundary conditions are sufficient for solving equations (4-5). The result is that the gas fraction f_g within the virial radius is 0.88 without preheating, and somewhat less when preheating is turned on.

The matter distribution in virialized clusters is well described by the NFW (Navarro, Frenk & White 1997) model as found from N-body Pure CDM simulations. Adiabatic hydrodynamical simulations without non-gravitational processes find gas density profiles quite similar to the NFW shape, except in the central regions (Voit et al. 2002), where the gas density levels off. When preheating is turned on, the inner gas density profile becomes even shallower and deviates more from the NFW shape. Since the gas is subdominant in mass, we neglect its effect on the distribution of dark matter. (Though it is found that gas will cause the dark matter halo to be slightly more concentrated; e.g. Lin et al. 2006.) For simplicity, here we assume the dark matter profile retains the NFW shape, i.e. $\rho_{\text{DM}}(r) = (1 - f_b)\rho_{\text{NFW}}(r)$. For a cluster virialized at redshift z with mass M_{vir} , its NFW density profile is given as,

$$\rho_{\text{NFW}}(r) = \frac{\delta_c \rho_c(z)}{(r/r_s)(1 + r/r_s)^2} \quad (7)$$

where ρ_c is the critical density of the universe, and δ_c and r_s are parameters determined from the concentration parameter $c \equiv r_{\text{vir}}/r_s$. We neglect the weak dependence of c on M_{vir} and z , and simply adopt a constant $c = 5$ in this paper. We identify clusters virialized at redshift z as spherical regions with mean density $\rho_{\text{vir}} = \Delta_v \rho_c(z)$, with Δ_v given as a fitting formula by Kuhlen et al. (2005, based on spherical collapse model),

$$\Delta_v = 18\pi^2 \Omega_m(z) [1 + a\Theta(z)^b], \quad (8)$$

where $\Theta(z) = \Omega_m^{-1}(z) - 1$, $\Omega_m(z)$ is the matter density normalized by $\rho_c(z)$, and $a = 0.432 - 2.001(|w(z)|^{0.234} - 1)$, $b = 0.929 - 0.222(|w(z)|^{0.727} - 1)$, with $w(z)$ the dark energy equation of state.

3. PREHEATING FROM THE L-T SCALING RELATIONS

Once the density, temperature and pressure profiles of the intracluster gas are specified, global properties, such as the X-ray luminosity, the emission-weighted temperature, and the Sunyaev-Zel'dovich decrement can be readily calculated. Here we compare predictions of the modified entropy model for the luminosity-temperature scaling relations with those inferred from X-ray observations. This choice is motivated by simplicity and robustness: the total luminosity (L) and temperature (T) can be inferred from observations without referring to a model for the intracluster gas. Comparisons to relations involving the mass of the cluster (such as the mass-temperature relation) are somewhat more direct from a theoretical point of view, but any such comparison

would, in any case, have to re-derive cluster masses, using information such as the observed X-ray surface brightness or temperature profiles, and using our own model, for a fair comparison with the data. We also emphasize that similar comparisons with SZ observables will contain valuable additional information (e.g. McCarthy et al. 2003; Younger et al. 2006), and should be possible soon with forthcoming data on cluster profiles from the Sunyaev-Zel'dovich Array (SZA) survey (Muchovej et al. 2007; Mroczkowski et al. 2007). We postpone such comparisons to future work.

The X-ray luminosity L of a cluster is calculated as,

$$L = \int dV \int d\nu n_e(r) n_H(r) \Lambda(T(r), \nu) \quad (9)$$

where $n_e = (1 - Y_{\text{He}} + \frac{Y_{\text{He}}}{2}) \frac{\rho_g}{m_p}$ is the number density of electrons, $n_H = (1 - Y_{\text{He}}) \frac{\rho_g}{m_p}$ is the number density of protons, and Λ is the cooling function, calculated by a Raymond-Smith (Raymond & Smith 1977) code with metallicity $Z = 0.3Z_{\odot}$. The integral is done over the cluster volume V and over frequency ν . The emission-weighted temperature is calculated as,

$$T_{\text{ew}} = \frac{\int dV \int d\nu \rho_g^2(r) \Lambda(T(r), \nu) T(r)}{\int dV \int d\nu \rho_g^2(r) \Lambda(T(r), \nu)} \quad (10)$$

The effect of preheating decreases the central density of the gas, but increases its temperature. The result is a lower luminosity and a higher T_{ew} ; the combined effect at fixed T_{ew} is a decrease in luminosity.

We compare our predictions to two flux-limited samples of X-ray clusters. One is the low-redshift Highest X-ray FLUX Galaxy Cluster Sample (HIFLUGCS) presented in Reiprich & Böhringer (2002), including 63 clusters whose mean redshift is $\langle z \rangle = 0.05$. The other is the high-redshift sample from the Wide Angle ROSAT Pointed Survey (WARPS) used in Maughan et al. (2006), including 11 clusters with a mean redshift of $\langle z \rangle = 0.8$. For each individual cluster, we predict its observed temperature as the one weighted by the bolometric emission,⁴ and compare the bolometric luminosity, calculated at this temperature using the preheating model, with the observed value. To quantify the goodness of fit of this comparison, we define the usual χ^2 statistic,

$$\chi^2 = \sum_{i=1}^N \frac{[\log L(T_i, z_i, K_0) - \log L_i]^2}{(\frac{\partial \log L}{\partial \log T} |_{T_i} \sigma_{\log T_i})^2 + \sigma_{\log L_i}^2}. \quad (11)$$

Here $\sigma_{\log T_i}$ and $\sigma_{\log L_i}$ denote the observational measurement errors of (the base 10 logarithm of) temperature and luminosity, i.e. $\sigma_{\log T_i} \equiv (\log e) \frac{\sigma_{T_i}}{T_i}$, and $\sigma_{\log L_i}$ is defined analogously (additional, intrinsic scatter in these quantities will be discussed below). We take $z_i, T_i, L_i, \sigma_{T_i}, \sigma_{L_i}$ directly from the published observational data, and L and $\frac{\partial \log L}{\partial \log T}$ are calculated from the preheating model. We fix the parameters of the background cosmology, adopting the flat Λ CDM model with the best-fit values from the *WMAP* 3-year results (Spergel et al.

2007), i.e. $(h, \Omega_m h^2, \Omega_b h^2, \sigma_8, n_s) = (0.73, 0.13, 0.022, 0.76, 0.96)$

Therefore, in this comparison, K_0 is the only free parameter to be determined by the fit (allowing variations in the cosmological parameters will be discussed below). We quote the best-fit entropy floor value by multiplying K , as defined in equation (1) above, by a constant factor of $(\mu m_p)^\gamma (n/n_e)^{\gamma-1}$, with $n = \frac{\rho_g}{\mu m_p}$. This is equivalent to redefining K as

$$K = \frac{T}{n_e^{\gamma-1}} \quad (12)$$

which is the definition widely used in the observational literature (e.g. Ponman, Cannon & Navarro 1999; Ponman, Sanderson, & Finoguenov 2003; Pratt & Arnaud 2005). For $\gamma = \frac{5}{3}$, commonly used units for the entropy defined above is keV cm², and 1 keV cm² corresponds to ejecting $0.036(1 + \delta_b)^{2/3}(1+z)^2 (\frac{\Omega_b h^2}{0.022})^{2/3}$ ev per particle to the fully-ionized plasma with overdensity δ_b and redshift z .

Note that the luminosity inferred from observations is cosmology-dependent, and since Reiprich & Böhringer (2002) and Maughan et al. (2006) adopt different values for the cosmological parameters, we re-scale their quoted luminosity (by the ratio of the luminosity distance-square) to our fiducial cosmology.

The above procedure, applied to the low-redshift HIFLUGCS clusters, yields the best-fit entropy floor of $K_0 = 295_{-5}^{+5} h^{-1/3}$ keV cm². We find a total $\chi^2 = 2293$ for this best fit model, or a χ^2 per degree of freedom (d.o.f.) of 37, indicating that the $L-T$ relation has additional intrinsic scatter (caused, possibly, by a cluster-to-cluster variation in the entropy floor itself; see discussion of scatter in § 5 below). For the high-redshift WARPS sample, we find the best fit K_0 to be $172_{-33}^{+35} h^{-1/3}$ keV cm². This fit has a total $\chi^2 = 7$, or a χ^2 per d.o.f. of 0.7.

The $L-T$ scaling relation predicted with the best-fit entropy floor at the average redshift of the HIFLUGCS clusters, $z = 0.05$, is shown as the solid curve in Figure 1, together with the re-scaled low- z data from Reiprich & Böhringer (2002). For reference, the figure shows the predicted $L-T$ relations without an entropy floor (dot-dashed curve) and with the lower K_0 inferred from the high- z sample (dashed curve). The comparison of the data with the $K_0 = 0$ curve clearly shows the need for the entropy floor, and the comparison with the $K_0 = 172 h^{-1/3}$ keV cm² curve shows that the observational data, especially of the 1-3 keV clusters, require that the entropy floor at $z = 0.05$ is higher than the best-fit value at $z = 0.8$.

The solid curve in Figure 2 shows the model prediction for the $L-T$ scaling relation with the best-fit entropy floor at the average redshift of the WARPS clusters, $z = 0.8$, together with the re-scaled data from Maughan et al. (2006). For reference, the figure again shows the predicted $L-T$ relations without an entropy floor (dot-dashed curve) and with the higher K_0 inferred from the low- z sample (dashed curve). The comparison of the data with the $K_0 = 0$ curve clearly shows the need for the entropy floor at high- z as well, and the comparison with the $K_0 = 295 h^{-1/3}$ keV cm² curve shows that the high- z clusters favor an entropy floor smaller than the best-fit value at low- z .

⁴ We find the difference of this temperature from that weighted by the band emission, which is actually observed, is less than 4%. We neglect this difference. We also checked the bias of the emission-weighted temperature when comparing to the observed spectroscopic temperatures (see § 6.3 below).

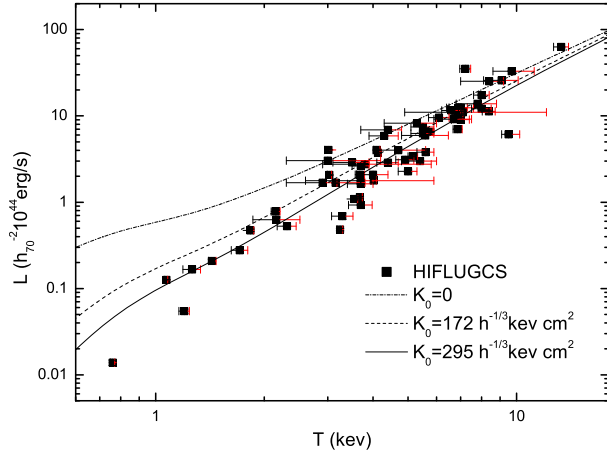


FIG. 1.— The $L - T$ scaling relation predicted by the preheating model with the best-fit entropy floor $K_0 = 295h^{-1/3}$ keV cm² at the average redshift $z = 0.05$ of the HIFLUGCS clusters (solid curve), together with data from Reiprich & Böhringer (2002), re-scaled to the WMAP 3-year cosmology adopted in our work. For reference, we show the $L - T$ relation at $z = 0.05$ predicted without an entropy floor ($K_0 = 0$; dot-dashed curve) and with the lower entropy inferred from the high- z sample ($K_0 = 172h^{-1/3}$ keV cm²; dashed curve; see Figure 2). Measurement errors on L are smaller than the size of the symbols.

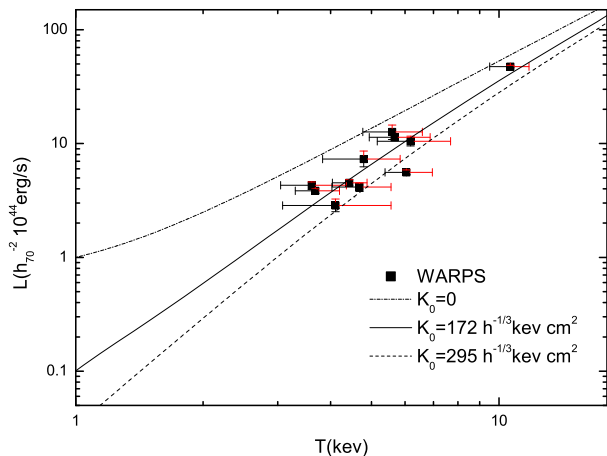


FIG. 2.— The $L - T$ scaling relation predicted by the preheating model with the best-fit entropy floor $K_0 = 172h^{-1/3}$ keV cm² at the average redshift $z = 0.8$ of the high-redshift WARPS clusters (solid curve), together with the re-scaled data from Maughan et al. (2006). For reference, we show the $L - T$ relation at $z = 0.80$ predicted without an entropy floor ($K_0 = 0$; dot-dashed curve) and with the higher entropy inferred from the low- z sample ($K_0 = 295h^{-1/3}$ keV cm²; dashed curve; see Figure 1).

A visual inspection of Figures 1 and 2 (“chi by eye”) indicates that the preheating model of a universal entropy floor, produced by energy input at an early epoch, can not fit the scaling relations of the low-redshift and high-redshift clusters simultaneously. (We discuss the significance of the detected evolution quantitatively below, in § 5.1 and in § 6.1.) It would be natural, in fact, for the entropy floor to increase with cosmic time, if the energy input is being continuously provided by stars and/or

AGN. Parameterizing the entropy evolution as a power-law in redshift,

$$K_0(z) = K_0(z=0)(1+z)^{-\alpha}, \quad (13)$$

we can convert the two best-fit values of K_0 for the two cluster samples at $z = 0.05$ and 0.8 to estimate $K_0(z=0) = 310h^{-1/3}$ keV cm² and $\alpha = 1$. For reference, this power-law is shown in Figure 4.

4. NUMBER COUNTS OF X-RAY CLUSTERS

The preheating model described above, with the power-law approximation for the evolution of the entropy floor, can successfully match the observed $L - T$ scaling relations. This model also predicts a deterministic relation between cluster mass M and both the temperature and luminosity. The mass function of dark matter halos is well understood from both analytic models (Press & Schechter 1974; Bond et al. 1991; Sheth & Torman 1999) and numerical simulations (Sheth & Torman 1999; Jenkins et al. 2001). It is therefore natural to compare model predictions to observed clusters counts as a function of either temperature T or luminosity L (or equivalently, flux f). Here we chose to compare the model predictions to the $\log N - \log f$ relation derived from the 158 deg² ROSAT PSPC survey by Vikhlinin et al. (1998). This sample is ideal for our purposes, since it is both large and deep enough to provide a good measurement of the counts to faint fluxes, where the effects of preheating are more pronounced.

We first use the best-fit cosmological model from the WMAP 3-year results, and calculate $\bar{N}(> f)$, the expected surface number density of clusters whose X-ray fluxes exceed f . The counts are calculated as

$$\bar{N}(> f) = \int_0^\infty dz \frac{d^2V}{dzd\Omega}(z) \int_{M_{180}(f,z)}^\infty \frac{dn}{dM}(M,z) dM, \quad (14)$$

where $d^2V/dz d\Omega$ is the comoving volume element, and $\frac{dn}{dM}$ is the cluster mass function. In this paper, we use the fitting formula given by Jenkins et al. (2001) for the SO(180) group finder of dark matter halos. The mass limit $M_{180}(f,z)$ is determined by first finding the virial mass $M_{\text{vir}}(f,z)$ of the cluster at redshift z that gives a flux f ; then converting it to $M_{180}(f,z)$ by extending the NFW profile of this cluster until the enclosed matter has a mean density of 180 times the background matter density at that time.

The results are shown as the dashed curve in Figure 3, together with the observational data from Vikhlinin et al. (1998). The figure shows that the WMAP 3-year cosmology, together with the preheating model that fits the $L - T$ scaling relations, underpredicts the cumulative number counts of X-ray clusters, especially at the low flux limits. Considering the sensitivity of the cluster number counts to σ_8 , it is natural to ask whether the discrepancy can be resolved by increasing the value of σ_8 and leaving all other parameters unchanged (clearly, variations in σ_8 will not modify the best-fit K_0 inferred from the scaling relations). We therefore vary σ_8 , and apply a χ^2 statistic to the 158deg² ROSAT PSPC data to find its best-fit value. We use

$$\chi^2 = \sum_i \frac{[\bar{N}_i(\sigma_8) - N_i]^2}{\sigma_{N_i}^2 + \frac{\bar{N}_i}{A}}, \quad (15)$$

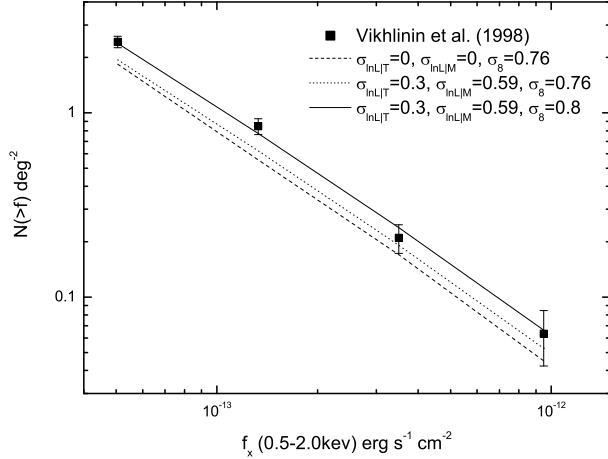


FIG. 3.— Cumulative number counts of galaxy clusters per deg^2 $N(>f)$ as a function of the X-ray flux f in the 0.5–2 keV soft X-ray band. Filled squares show data from Vikhlinin et al. (1998). The dashed curve shows predictions using the *WMAP* 3-year cosmology (in particular, $\sigma_8 = 0.76$), and the $L-M$ relation calculated from the preheating model without consideration of any intrinsic scatter ($\sigma_{\ln L|T} = \sigma_{\ln L|M} = 0$). The dotted curve corresponds to the case with intrinsic scatters of $\sigma_{\ln L|T} = 0.3$ and $\sigma_{\ln L|M} = 0.59$. The solid curve is similar to the dotted curve, except it is calculated with a higher $\sigma_8 = 0.8$, which gives the best agreement with the data when scatter is included.

where i labels independent flux bin, A is the survey area. We include a simple Poisson error (uniform sky coverage at all flux limits) in the calculation of the variance in addition to the measurement error. We find the best-fit value of $\sigma_8 = 0.82 \pm 0.02$, which is larger than the *WMAP* 3-year best-fit value $\sigma_8 = 0.76 \pm 0.05$ (in the presence of scatter, our best-fit is reduced to $\sigma_8 = 0.80 \pm 0.02$; see below).

5. THE EFFECTS OF INTRINSIC SCATTER

In the above two sections, we assumed that clusters at redshift z with fixed virial mass M_{vir} have temperatures and luminosity exactly as predicted by the preheating model. In reality, deviations from spherical symmetry, as well as cluster-to-cluster variations in non-adiabatic processes, will lead to non-negligible scatter in these two quantities. For flux-limited surveys, such scatter will cause the observed scaling relations to deviate from the true ones (Stanek et al. 2006; Nord et al. 2007), and the counts to deviate from those of equivalent mass-limited samples without scatter. To make our analysis more realistic, it is necessary to take these effects into account. In this section, we repeat the calculations in the above two sections, but we include intrinsic scatter, which we model separately in the $L-T$ and $L-M$ relations.

5.1. Scatter in the $L-T$ Relation

At a given redshift z , the joint probability distribution for L and T of a cluster with fixed M_{vir} may be conveniently modeled as a bivariate log-normal distribution $P(L, T|M_{\text{vir}})$, with the logarithmic means determined by M_{vir} (Nord et al. 2007). Convolved with the cluster mass function, this can be used to predict the probability distribution of luminosity for clusters at fixed temperature T . For a flux-limited sample, the average and variance

of L for these clusters can also be predicted. Here, since we care only about the final $L-T$ scaling relation, for simplicity, we assume that $P(L|T)$, the probability distribution function of L for clusters at fixed T is log-normal,

$$P(L|T)dL = \frac{1}{\sqrt{2\pi}\sigma_{\ln L|T}} \exp\left(-\frac{(\ln L - \overline{\ln L})^2}{2\sigma_{\ln L|T}^2}\right) d\ln L. \quad (16)$$

Given that the log-normal shape of $P(L, T|M)$ is not particularly well justified to begin with, and that our results are essentially more sensitive to the width of the $P(L|T)$ distribution than its detailed shape, we regard this as a sensible approach. The logarithmic mean $\overline{\ln L}$ in equation (16) is taken to be the logarithm of the luminosity predicted by the preheating model for a cluster that has temperature T according to the same model. The scatter $\sigma_{\ln L|T}$ is taken to be a constant. Here we choose it to be 0.3, which is close to the value ~ 0.4 expected for current flux-limited [$f(0.1-2.4\text{keV}) \sim 3 \times 10^{-12} \text{erg/s/cm}^2$] samples. In particular, Nord et al. (2007) derive this value by assuming a bivariate log-normal distribution of $P(L, T|M)$, with intrinsic scatters $\sigma_{\ln L|M} = 0.59$, $\sigma_{\ln T|M} = 0.1$, power-law relations between the means, and a positive correlation between $\ln L$ and $\ln T$.

For a flux-limited survey with a threshold f_{min} in the observer rest frame energy band $[\nu_1, \nu_2]$, the log mean luminosity of detectable clusters at fixed temperature T is given by,

$$\langle \ln L \rangle(T) = \overline{\ln L} + \sigma_{\ln L|T} \sqrt{\frac{2}{\pi}} \frac{\exp(-x_{\text{min}}^2)}{\text{erfc}(x_{\text{min}})}, \quad (17)$$

where erfc is the complimentary error function, $x_{\text{min}} = \frac{\ln L_{\text{min}} - \overline{\ln L}}{\sigma_{\ln L|T}}$, and L_{min} is the luminosity corresponding to the flux threshold, $L_{\text{min}} = 4\pi d_L^2(z) f_{\text{min}} / K(T, z)$. Here $d_L(z)$ is the luminosity distance, K is the ratio of the X-ray emission in the energy band $[\nu_1(1+z), \nu_2(1+z)]$ (cluster rest frame) to the bolometric luminosity, and is calculated by the preheating model for the same cluster when we calculate $\overline{\ln L}$. Clusters with luminosity below L_{min} are not included in the average. So, $\langle \ln L \rangle$ is larger than that for the complete sample (the so-called Malmquist bias). The variance for the log of the luminosity for the flux-limited sample can be calculated similarly,

$$\langle (\ln L - \langle \ln L \rangle)^2 \rangle(T) = \sigma_{\ln L|T}^2 \times \left[1 + \frac{2}{\sqrt{\pi}} \frac{x_{\text{min}} \exp(-x_{\text{min}}^2)}{\text{erfc}(x_{\text{min}})} - \frac{2}{\pi} \frac{\exp(-2x_{\text{min}}^2)}{\text{erfc}^2(x_{\text{min}})} \right]. \quad (18)$$

Note that equations (17) and (18) have manifestly correct limiting behaviors: in the limit $L_{\text{min}} \rightarrow 0$, $\langle \ln L \rangle \rightarrow \overline{\ln L}$ and $\langle (\ln L - \langle \ln L \rangle)^2 \rangle \rightarrow \sigma_{\ln L|T}^2$; whereas in the limit $L_{\text{min}} \rightarrow \infty$, we have $\langle \ln L \rangle \rightarrow L_{\text{min}}$ and $\langle (\ln L - \langle \ln L \rangle)^2 \rangle \rightarrow \frac{\sigma_{\ln L|T}^2}{x_{\text{min}}^2} \rightarrow 0$.

To take into account the above, we modify the calculation of the χ^2 statistic for the two flux-limited cluster samples. Specifically, in equation (11), we replace the average $\log L(T_i, z_i, K_0)$ by $\langle \ln L \rangle(T_i, z_i, K_0) \times (\log e)$, and the variance $(\frac{\partial \log L}{\partial \log T}|_{T_i} \sigma_{\log T_i})^2$ by $\langle (\ln L -$

$(\ln L)^2)(T_i, z) \times (\log e)^2$. Measurement errors in the temperature may further modify the average and variance of the i^{th} cluster's luminosity; here, we include this effect approximately by simply adding a term $\left(\frac{\partial(\ln L)}{\partial \ln T} \sigma_{\log T_i}\right)^2$ to the intrinsic variance.

With these alterations of the χ^2 statistic, we find that the best-fit entropy floor K_0 for the low-redshift HIFLUGCS clusters is increased to $327_{-19}^{+20} h^{-1/3}$ keV cm² (with the χ^2 per d.o.f of 2.2), and the best-fit K_0 for the high-redshift WARPS clusters is increased to $209_{-60}^{+66} h^{-1/3}$ keV cm² (with the χ^2 per d.o.f of 0.5).⁵ Since Malmquist bias shifts the average luminosity to a larger value, more entropy is needed to bring the model prediction to agree with the observations (see § 6.6 for more discussions on this), but the increase is only $\approx 10 - 20\%$. More importantly, however, we see that the significance of the difference in K_0 between the high- and low-redshift samples is reduced, but remains at the interesting level of $(327 - 209)/(\sqrt{19^2 + 66^2}) \approx 1.7\sigma$. (See § 6.1 for more about this.) We find that the power-law approximated evolution of the entropy floor changes to $K_0(z) = 341(1+z)^{-0.83} h^{-1/3}$ keV cm².

5.2. Scatter in the $L - M$ Relation

In this section, as before, we assume that the bolometric luminosity L for clusters with virial mass M_{vir} at redshift z has a log-normal probability distribution,

$$P(L|M_{\text{vir}}, z)dL = \frac{1}{\sqrt{2\pi}\sigma_{\ln L|M}} \exp\left(-\frac{(\ln L - \overline{\ln L})^2}{2\sigma_{\ln L|M}^2}\right) d\ln L. \quad (19)$$

The log mean $\overline{\ln L}$ is calculated as the logarithm of the luminosity predicted for the cluster by the preheating model with the evolving entropy floor found from § 5.1. The scatter is taken to be a constant; we adopt the value $\sigma_{\ln L|M} = 0.59$ derived by Stanek et al. (2006) from matching the predicted cluster counts to the REFLEX survey results (Böhringer et al. 2004).

The fraction of clusters with flux above f , or luminosity above L_{min} , is then simply

$$P(> f|M_{\text{vir}}) = \frac{1}{2} \text{erfc}(x_{\text{min}}), \quad (20)$$

where L_{min} and x_{min} are calculated as in § 5.1. Finally, the number counts are given by

$$\bar{N}(> f) = \int dz \frac{d^2 V}{dz d\Omega}(z) \int \frac{dn}{dM}(M, z) P(> f|M_{\text{vir}}, z) dM. \quad (21)$$

Note M , the mass of the cluster employed in the mass function, is defined by an overdensity of 180 of the background matter density, different from M_{vir} . As before, the NFW profile is used to convert M_{vir} to M . The counts predicted in this model with scatter are shown as the dotted curve in Figure 3. The difference from the original calculation, assuming no intrinsic scatter (dashed curve), is relatively small. Although a non-zero $\sigma_{\ln L|M}$, by itself, tends to significantly increase the number counts, we are also allowing the log mean luminosity

$\overline{\ln L}$ (at fixed M) to change. As explained in the preceding subsection, a non-zero $\sigma_{\ln L|T}$ necessitates more entropy in order to match the $L - T$ scaling relations, and tends to reduce $\overline{\ln L}$ (at fixed T , and also at fixed M), and hence to decrease the number counts. The combination of these two effects is that $\bar{N}(> f)$ increases, but only by a relatively small factor ($\sim 20\%$).

By repeating the analysis as is done at the end of § 4, we find that when all other cosmological parameters are kept fixed at the best-fit values from the *WMAP* 3-year results, the preheating model that agrees with the $L - T$ scaling relations at both low and high redshift reduces the best-fit value of σ_8 by a small amount, from $0.82_{-0.02}^{+0.02}$ to $0.80_{-0.02}^{+0.02}$ (see Figure 3). The latter value still exceeds the best-fit value from the *WMAP* 3-year data, but becomes marginally consistent with their 1σ error. We also note that our best-fit $\sigma_8 = 0.80$ agrees well with the value found by Lesgourgues et al. (2007) from a combined analysis of Lyman- α forest, 3D weak lensing and the *WMAP* year three data.

6. DISCUSSION

In this section, we discuss, quantitatively, a range of issues that should help understand our results and assess their robustness.

6.1. Significance of the Inferred Entropy Evolution

Perhaps our most interesting result is the increase in the entropy floor from the $z \sim 0.8$ to the $z \sim 0.05$ cluster sample, and therefore here we discuss the statistical significance of this difference. In our analysis above, we have assumed a constant (not evolving) intrinsic scatter $\sigma_{\ln L|T}$, adapted from the work of Nord et al. (2007), resulting in a $\approx 1.7\sigma$ detection for the difference in the entropy floor values at $z = 0.8$ and $z = 0.05$ (see § 5.1 above). In reality, the measurement errors of the low- z cluster sample are much smaller than those of the high- z sample, and the intrinsic scatter can, in fact, be inferred self-consistently from the $L - T$ relation we fit. Here we repeat the analysis in § 5.1, but we allow the scatter $\sigma_{\ln L|T}$ to vary, and attempt to adjust its value to find a χ^2 per degree of freedom of unity, for both cluster samples. We find that the low- z sample then requires a scatter of $\sigma_{\ln L|T} = 0.49$, which is larger than our adopted value. Using this larger scatter shifts the best-fit entropy level to $372_{-36}^{+37} h^{-1/3}$ keV cm². For the high- z sample, we find that the measurement errors are so large that the best-fit model has a χ^2 per d.o.f is less than 1 (≈ 0.7) even in the absence of any intrinsic scatter. We conclude that the current data can not yet be used to establish evidence for any intrinsic scatter in the high- z sample. The best motivated statistical comparison, then, is between the best-fit K_0 we obtain for the low- z sample with $\sigma_{\ln L|T} = 0.49$, and the best-fit value for the high- z sample obtained with $\sigma_{\ln L|T} = 0$ ($172_{-33}^{+35} h^{-1/3}$ keV cm², see § 3). This implies a significance of the difference between the best-fit values of $(372 - 172)/(\sqrt{37^2 + 35^2}) \approx 4\sigma$ (with the best-fit power-law evolution changing to $K_0(z) = 398(1+z)^{-1.43} h^{-1/3}$ keV cm²). Clearly, better temperature measurements for the high- z clusters would help determine whether the intrinsic scatter evolves, which would be important to validate this result.

⁵ Two clusters in the high-redshift WARPS sample are removed here because they fall below the nominal flux threshold given in Maughan et al. (2006).

The entropy floor has a larger impact on the smallest clusters, and one may wonder to what extent the inferred entropy floor is driven by the two low-temperature clusters in Figure 1 that lie visibly below the best-fit relation. When we omit these two clusters and repeat our analysis with the rest of the HIFLUGCS sample, we find that the best-fit entropy floor decreases by 7%, from $295^{+5}_{-5} h^{-1/3}$ keV cm² when ignoring intrinsic scatter in the analysis, by 12%, from 327^{+20}_{-19} to $287^{+22}_{-20} h^{-1/3}$ keV cm², when including intrinsic scatter ($\sigma_{\ln L|T} = 0.3$), and also by 12%, from 372^{+37}_{-36} to $329^{+40}_{-39} h^{-1/3}$ keV cm², when including a larger intrinsic scatter ($\sigma_{\ln L|T} = 0.49$). The 4σ significance of difference claimed above now reduces to 3σ .

Finally, we use an alternative statistic to assess the significance of the difference between the high- z and low- z entropy floors. We derive the entropy floor K_0 for each individual cluster in the two samples by simply setting $L(T_i, z_i, K_0) = L_i$ (following the notation in § 3). This results in a range of K_0 values, shown by the symbols in Figure 4, which can be used to construct two separate K_0 -distributions, for the high- z and low- z samples. We then apply a Kolmogorov-Smirnov (KS) test to the two K_0 -distributions. We find $D = 0.4$ and a P-value of 0.07, which makes it unlikely that the two sets of K_0 values were drawn from the same underlying distribution. Unfortunately, this test remains inconclusive at present, since, as mentioned above, the observational errors on the temperature are much larger in the high- z sample than in the low- z sample, and this difference alone introduces a difference in the inferred K_0 distributions. Furthermore, the intrinsic scatter may evolve between the two redshifts due to reasons unrelated to the entropy floor. Indeed, this is suggested by the presence of negative K_0 values in the low- z sample, which presumably arises from un-modeled processes that brighten some clusters' X-ray emission (e.g. cooling cores). In order to conclude that the KS tests detects a true evolution (either in entropy, or in some other process modifying the luminosity distribution at fixed T), we would have to explicitly model the observational errors, which is not yet warranted, given the large errors in the high- z sample.

6.2. Evolution of the X-ray Scaling Relations

Our analysis requires evolution in the entropy floor, which also predicts a specific evolution in the $L - T$ scaling relation. In this section, we compare these evolutions with those derived from observations in previous work. A particularly relevant study is by Ettori et al. (2004, hereafter E04), which examines the evolution of the entropy K inferred from the X-ray scaling relation, with K measured at $0.1R_{200}$. They find the entropy K at fixed temperature evolves as $(1+z)^{0.3}/E_z^{4/3}$, corresponding, from $z = 0.8$ to $z = 0.05$, to a 50% increase, which appears, naively, to be in good agreement with our finding. However, we caution that E04 measure K at $0.1R_{200}$, which may include a contribution from gravitational shock heating, especially in higher-mass clusters, and therefore will not correspond directly to the preheating entropy we derive (furthermore, the β -model density profile assumed in E04 differs from the one in our model).

Our high- z sample is taken from Maughan et al. (2006),

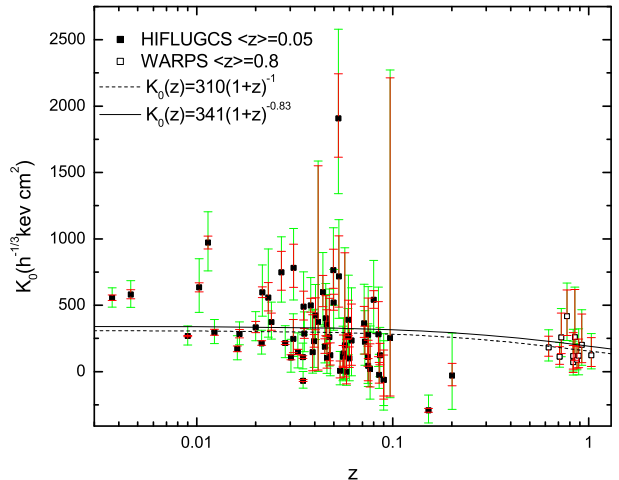


FIG. 4.— The entropy floor inferred for individual clusters in the HIFLUGCS and high-redshift WARPS samples, shown against the cluster's redshift. The narrower (red) error bars are obtained by allowing the predicted luminosity for the cluster to vary within the 1σ regions allowed by observational errors, while the wider (green) ones are obtained by additionally including a constant intrinsic scatter in luminosity at fixed temperature $\sigma_{\ln L|T} = 0.3$. The curves are the power-law evolution for the entropy floor obtained by without taking into account of the intrinsic scatter (dashed curve) and with the intrinsic scatter of $\sigma_{\ln L|T} = 0.3$ (solid curve).

which also analyzed the evolution of the $L - T$ relation, and found that this evolution is consistent with the expectation in self-similar models (with no preheating). How can this be reconciled with our results? We first note that the high- z sample in Maughan et al. (2006) includes only clusters with $T > 3$ keV, and that their inferred evolution relates to the normalization of the best-fit power-law relations (whereas our $L - T$ relations are not power-laws). For a clear illustration of how the two results can be reconciled, we return to our calculations without intrinsic scatter. In Figure 5, we reproduce the mean $L - T$ relations from Figure 1 and Figure 2, and overlay the six model curves in a single figure. Note that the lowest solid curve and the middle dashed curve are predicted at our best-fit entropy levels for the low- z and high- z sample, respectively. Comparing these two curves with those predicted with $K_0 = 0$, we find our evolving entropy floor predicts a self-similar-like evolution for the $L - T$ scaling relations when $T > 3$ keV, in agreement with Maughan et al. (2006). This figure also clearly shows that a constant but non-zero K_0 can not mimic a self-similar-like evolution.

This can be explained by the following: for clusters at the same redshift, the same entropy level (K_0) affects the low-temperature clusters more than it does the high-temperature ones, because the latter have larger characteristic (gravitational-heated) entropy. (This, of course, is well known, and it is the effect that leads to a larger fractional reduction in the luminosity for the low- T systems, steepening the $L - T$ scaling relations.). Similarly, for clusters with the same T but at different redshifts, a constant entropy level leads to a larger fractional reduction in the luminosity for the higher redshift clusters, because they have larger characteristic density and a smaller entropy. As a result, maintaining the self-

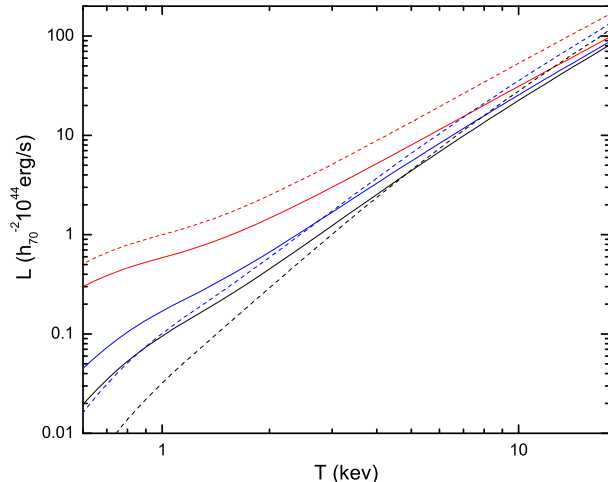


FIG. 5.— $L - T$ scaling relations predicted by the preheating model at different redshifts and different entropy levels. Solid lines are at redshift $z = 0.05$, and dashed lines are at redshift $z = 0.8$. In both set of lines, from bottom to up the entropy floors are set at 295, 172, $0 h^{-1/3} \text{ keV cm}^2$. The curves are reproduced from Figures 1 and 2.

similar-like evolution requires less entropy at higher redshift.

Provided $T \propto M_{\text{vir}}^{2/3} \rho_{\text{vir}}(z)^{1/3}$, we have $K_{\text{vir}} \propto T \rho_{\text{vir}}(z)^{-2/3}$; to maintain self-similar evolution of L at fixed T , we would need $K_0 \propto \rho_{\text{vir}}(z)^{-2/3}$. Taking $K_0 = 295$ at $z = 0.05$, this requires $K_0 = 136$ at $z = 0.8$, 20% smaller than our best-fit value at this redshift. This indicates that the evolution of our $L - T$ scaling relation is not exactly self-similar, but a little shallower. Figure 4 in Maughan et al. (2006) is indeed consistent with this small deviation from self-similarity.

6.3. Bias of the Emission-weighted Temperature

In our analysis above, we have compared the predicted emission-weighted temperature T_{ew} for a cluster to its observational counterpart. Since the latter is generally obtained by fitting a thermal model to the observed spectrum, in general the former is a biased estimator. In particular, Mazzotta et al. (2004) have demonstrated that T_{ew} always overestimates the spectroscopic temperature if the cluster has a complex multi-temperature thermal structure. They proposed alternatively using a so-called spectroscopic-like temperature T_{sl} , which they found to be within a few percent of the actual spectroscopic temperature, measured for simulated clusters hotter than 2–3 keV. To quantify how the bias in T_{ew} affect our results, we adopted the formula for T_{sl} from Mazzotta et al. (2004) and repeated our calculations. We find T_{sl} is larger than T_{ew} by around 10%. The result is that the best-fit entropy level shifts to a higher value: from 327 to $420 h^{-1/3} \text{ keV cm}^2$ for the HIFLUGCS sample, and from 209 to $287 h^{-1/3} \text{ keV cm}^2$ for the WARPS sample, giving the evolution of $K_0(z) = 436(1+z)^{-0.71} h^{-1/3} \text{ keV cm}^2$. (The effects of intrinsic scatter in $\sigma_{\ln L|T}$ and Malmquist bias are included in these results, as in § 5.1.)

6.4. Parameter Degeneracies

An obvious issue, even within the context of the simple model adopted in our study, is that of parameter degeneracies. A full multi-dimensional degeneracy study is left for future work; here we examine only the variations between parameters that we expect may have the largest effect on our conclusions.

Overall degeneracy between η , K_0 , and σ_8 . In our fiducial model, we have included 20% non-thermal pressure support (i.e. $\eta = 0.8$). This choice is motivated by simulations that reveal turbulent motions in the intracluster gas (Norman & Bryan 1999; Faltenbacher et al. 2005; Younger & Bryan 2007). Including turbulent support in the analytical model is indeed necessary in order to reproduce in detail the density and temperature profiles for the intracluster gas in simulations with preheating (Younger & Bryan 2007). There is also direct observational evidence for turbulence in the Coma cluster (Schuecker et al. 2004). In addition to turbulence, however, relativistic particles accelerated by cosmic shocks or other mechanisms can provide further pressure support for the intracluster gas (Miniati 2005). In order to account for the possibility of such an additional pressure component, we repeated the analysis of the previous sections, but changed the value of η from 0.8 to $\eta = 0.7$. This new calculation serves, more generally, to quantify the impact of uncertainty in the non-thermal pressure component on our result.

We find that more non-thermal pressure support decreases both the density and the temperature for a cluster at fixed mass, and decreases both its L and T_{ew} . However, at a fixed T_{ew} , we find that L is slightly increased. As a result, in order to reproduce the observed $L - T$ scaling relations, more entropy is needed (both at low and high redshift). We find the best-fit evolving entropy floor is changed to $K_0(z) = 381(1+z)^{-0.84} h^{-1/3} \text{ keV cm}^2$. After preheating is included, keeping the WMAP 3-year cosmological parameters fixed, the model underpredicts the number counts even more, as a result of the decreased luminosity at fixed virial mass. Treating σ_8 as a free parameter, we find the best-fit value is increased to $\sigma_8 = 0.86$. (Intrinsic scatters are included in the analysis as in § 5.) According to this analysis, non-thermal pressure support is degenerate with both the entropy floor and the normalization of the power spectrum: a 50% increase in non-thermal pressure results in a 8% increase in σ_8 and an $\approx 12\%$ increase in K_0 (with virtually no effect on the slope of the entropy-evolution).

Degeneracy between K_0 and σ_8 from dN/df . We found above that if the entropy floor K_0 is fitted from the scaling relations alone, then the best-fit σ_8 is somewhat higher than the preferred WMAP 3-yr value. It is interesting to quantify the degeneracy between K_0 and σ_8 from the counts alone – in particular, to see how large a change in K_0 is required if one insists on the preferred WMAP 3-yr value of $\sigma_8 = 0.76$. We fix the power-law form of the evolution, $K_0(z) = K_0(z=0)(1+z)^{-0.83}$ (and include a scatter $\sigma_{\ln L|M} = 0.59$, as before), and compute the χ^2 statistic from the number counts, varying $K_0(z=0)$ and σ_8 simultaneously. The results are shown in Figure 6. As this figure reveals, the best-fit K_0 varies monotonically with σ_8 , by a factor of ≈ 2 over the range $0.7 < \sigma_8 < 0.85$. Also, the best-fit value for σ_8 from the $L - T$ relation is significantly discrepant (at the $\approx 2\sigma$

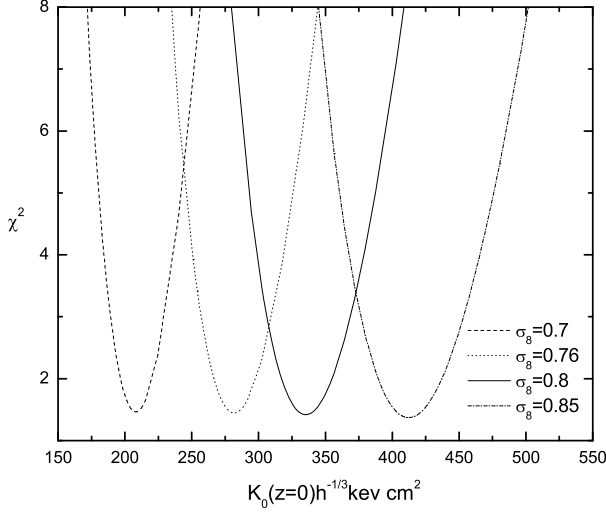


FIG. 6.— Constraints from the observed X-ray cluster number counts (Vikhlinin et al. 1998) on the normalization of the evolving entropy floor $K_0(z) = K_0(z=0)(1+z)^{-0.83}h^{-1/3}$ keV cm², for different fixed values of σ_8 . The y -axis shows the χ^2 , computed from equation (15) (Predictions for the counts include the intrinsic scatter of $\sigma_{\ln L|M}$).

level) from the central *WMAP* 3-yr value of $\sigma_8 = 0.76$; this discrepancy can be eliminated by increasing K_0 by $\approx 20\%$.

Degeneracy between Ω_m and σ_8 . Cluster number counts produce a well-known degeneracy between Ω_m and σ_8 , approximately of the form $\sigma_8 \Omega_m^{0.5} = \text{constant}$ for shallow X-ray counts (e.g., Eke, Cole & Frenk 1996; Bahcall & Fan 1998).

To examine the impact of uncertainty in Ω_m on our results, we changed Ω_m from 0.24 to 0.30 (corresponding to change $\Omega_m h^2$ from 0.13 to 0.16). We otherwise fix the *WMAP* 3-year cosmological parameters, and re-fit the $L-T$ scaling relations. We find that the best-fit evolving entropy floor is decreased significantly, by $\sim 40\%$, to $K_0(z) = 194(1+z)^{-0.72}h^{-1/3}$ keV cm². This can be understood easily: increasing Ω_m decreases the cosmic baryon fraction. For a cluster with fixed (M_{vir}, z) , the baryon content is therefore decreased. This reduces its luminosity with the same entropy floor. On the other hand, the temperature is essentially unchanged. The net result is that the normalization of the $L-T$ relation is reduced, and less entropy is needed to bring it into agreement with the observations.

The model with the best-fit entropy floor is then found to *over* predict the X-ray cluster counts. This is mostly due to the increase in the underlying mass function dn/dM , though we also find increased detection probability for the low mass clusters at a given flux limit, which may be caused by increased mean luminosity, reduced luminosity distance, etc. Allowing σ_8 to vary, we find the best-fit value of $\sigma_8 = 0.66$. This value is smaller than $\sigma_8 = 0.72$, the value expected from the usual degeneracy $\sigma_8 \Omega_m^{0.5}$. (Intrinsic scatters are included in the analysis as we do in § 5.)

6.5. Which Clusters Are Responsible for the Number Counts Constraints?

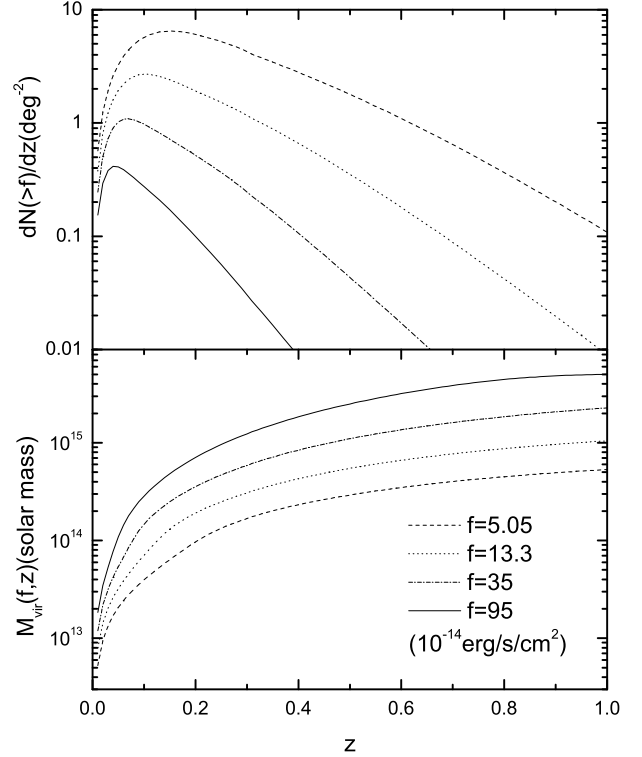


FIG. 7.— The upper panel shows the redshift distribution of the cumulative number density of the X-ray clusters, predicted at the flux thresholds of the four data points displayed in Figure 3. Our best-fit preheating model is used with $K_0(z) = 341(1+z)^{-0.83}h^{-1/3}$ keV cm² and the *WMAP* 3-year cosmology, except with $\sigma_8 = 0.8$. The lower panel shows the mean mass corresponding to the four different flux thresholds, as a function of redshift.

It is useful to know, within our model, the masses and redshifts of clusters that dominate the number counts. In Figure 7, we show $dN(>f)/dz$ and $M_{\text{vir}}(f, z)$ at the four different flux thresholds we utilized from Vikhlinin et al. (1998). The constant intrinsic scatter of $\sigma_{\ln L|M}$ is adopted in the calculation of dN/dz , so $M_{\text{vir}}(f, z)$ is actually the mass of the clusters that have 50% detection probability. As this figure shows, most of the clusters are in the range $0.05 \lesssim z \lesssim 0.15$ and have masses of $\approx 0.5 - 2 \times 10^{14} M_\odot$. The results also show that we have included some low mass clusters (few $\times 10^{13} M_\odot$), but the number of these clusters only constitute a small fraction of the total, e.g. at $f = 5.05 \times 10^{-14}$ erg/s/cm², the fraction of clusters with $M_{\text{vir}} < 5 \times 10^{13} M_\odot$ is $\sim 13\%$.

6.6. The Impact of Malmquist Bias on the Entropy Floor

As an “academic exercise”, it is useful to assess the impact of incorporating a flux limit, and the corresponding Malmquist bias, into our analysis. For this purpose, we assume that there is an intrinsic scatter of $\sigma_{\ln L|T} = 0.3$ as before, but we do *not* apply any flux limit (this corresponds to setting $x_{\text{min}} \rightarrow -\infty$ in Section 5.1). The best-fit entropy floor is found to be $333h^{-1/3}$ keV cm² for the HIFLUGCS clusters and $174h^{-1/3}$ keV cm² for the WARPS clusters (the two clusters with fluxes below the claimed flux limit are excluded, for the purpose of

fairly comparing with the results that take into account of the effect of the flux limit). The entropy evolution is now $K_0(z) = 353(1+z)^{-1.2}h^{-1/3} \text{ keV cm}^2$.

Compared with the results with no intrinsic scatter, the entropy levels favored by these two cluster samples both increase. This increase is caused by the constant intrinsic scatter added to the denominator in the calculation of the χ^2 analysis, which changes the relative weight of each cluster (more specifically, reducing the down-weighting of the (small) clusters that require a higher entropy floor).

Compared with the results that include the intrinsic scatter and also apply the survey flux limits, the entropy level for the HIFLUGCS sample increases a little, while for the WARPS sample, it decreases. Overall, the impact of the flux limit is surprisingly modest. One naively expects that the clusters that are most important for determining the best-fit value for the entropy floor are the smallest ones, i.e. those just above the detection threshold, which are most susceptible to bias effects. In particular, a naive expectation is that this bias will increase the average luminosity, and will require a larger entropy floor. It is therefore worth understanding the relative insensitivity of our results to imposing a flux limit.

The effects of applying the flux limits have been analyzed in Section 5.1: in addition to increasing the average luminosity, it also decreases the intrinsic scatter. The former effect shifts the best-fit entropy to a higher value, while the latter preferentially increases the value of χ^2 at a larger entropy floor, and effectively shifts the best-fit entropy level to a lower value. Depending on the competition between these two effects, the net result may be either a larger or a smaller value for the best-fit entropy floor. To clarify this competition, we perform an intermediate calculation, in which the effect of the flux limit is included only on the average luminosity (i.e. artificially ignoring the corresponding reduction in the scatter). We find the HIFLUGCS clusters now favor $K_0 = 411h^{-1/3} \text{ keV cm}^2$, and the WARPS clusters favor $K_0 = 251h^{-1/3} \text{ keV cm}^2$. These values are much larger than the values obtained by assuming there are no flux limits, demonstrating that the robustness of the inferred entropy floor results from the above-mentioned cancellation. We conclude that *provided the intrinsic scatter is known a-priori (before a flux limit is applied)*, the effect of Malmquist bias on the inferred entropy floor is small.

6.7. Predictions for the SZ Decrement

As mentioned above, our model fully determines other possible observables, such as those that can be measured with the SZ effect. In Figure 8, we plot predictions for the $Y_{2500} - T$ scaling relation, together with the data from Bonamente et al. (2007) (see also Reese et al. (2002); McCarthy et al. (2003); Bonamente et al. (2006); LaRoque et al. (2006) for further discussions of SZ decrements). Here Y_{2500} is the integration of the usual Compton parameter over the solid angle extended by the cluster within the projected radius of r_{2500} (the radius that gives a mean enclosed density of 2500 times of the critical density), and T is the (X-ray) emission-weighted temperature as before. The solid curve corresponds to our preheating model with the best-fit evolving entropy floor, and the dashed curve, for reference, shows the pre-

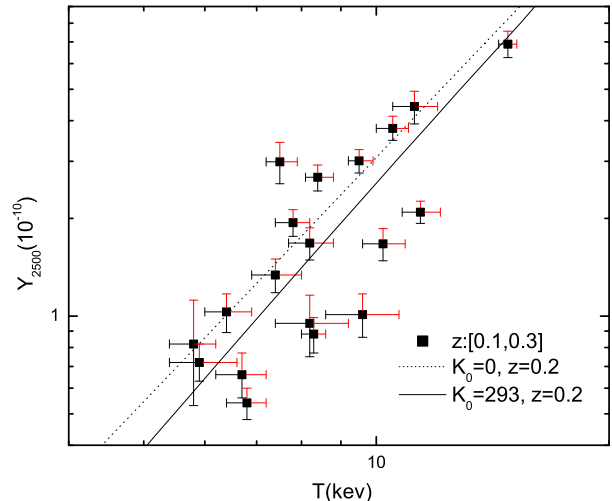


FIG. 8.— The $Y_{2500} - T$ Sunyaev-Zel'dovich scaling relations predicted by the preheating model with the best-fit evolving entropy floor given by $K_0(z) = 341(1+z)^{-0.83}h^{-1/3} \text{ keV cm}^2$ (solid curve), and without an entropy floor (dashed curve) at redshift $z = 0.2$. The points with error bars are data from Bonamente et al. (2007) for clusters within the redshift range of $[0.1, 0.3]$.

diction in model without preheating. Both are made at the mean redshift of the data $z = 0.2$. A visual inspection of the dashed and solid curves (“chi by eye”) indicates the data requires preheating, and that the entropy level we found from the X-ray scaling relations roughly agrees with the data. A thorough investigation of the SZ profiles, compared with the X-ray profiles, is likely to yield interesting new constraints on preheated cluster models (e.g. Cavaliere, Lapi, & Rephaeli 2005), but we leave this to future work.

6.8. Moore vs. NFW Dark Matter Profiles

High-resolution numerical simulations suggest that the dark matter distribution in the central regions of virialized haloes is significantly steeper than the NFW shape (Moore et al. 1998; Klypin et al. 2001). To examine the dependence of our results on possible variations of the dark matter profile, here we adopt

$$\rho(r) = \frac{\delta_c \rho_c(z)}{(r/r_s)^{1.5}(1+r/r_s)^{1.5}} \quad (22)$$

with a fixed concentration parameter $c = 4$, and recompute our results. We find that the steeper dark matter profile gives a higher central density and temperature for the intracluster gas, so at a fixed M_{vir} , both L and T are increased, but at a fixed T , the luminosity is decreased. As a result, less entropy is needed for the preheating model to agree with the observed $L - T$ scaling relations. We find the favored evolving entropy floor is $K_0(z) = 265(1+z)^{-0.75}h^{-1/3} \text{ keV cm}^2$. With the WMAP 3-year best-fit cosmology, the model overpredicts the number density of the X-ray clusters, and the best-fit σ_8 is lowered to 0.74. (Intrinsic scatters are included in the analysis as we do in § 5.)

We also use this steeper dark matter profile to predict the SZ observables y_0 and Y_{2500} . We find, similarly to L and T , that at a fixed M_{vir} , both y_0 and Y_{2500} are increased; at a fixed T , however Y_{2500} is decreased, but y_0

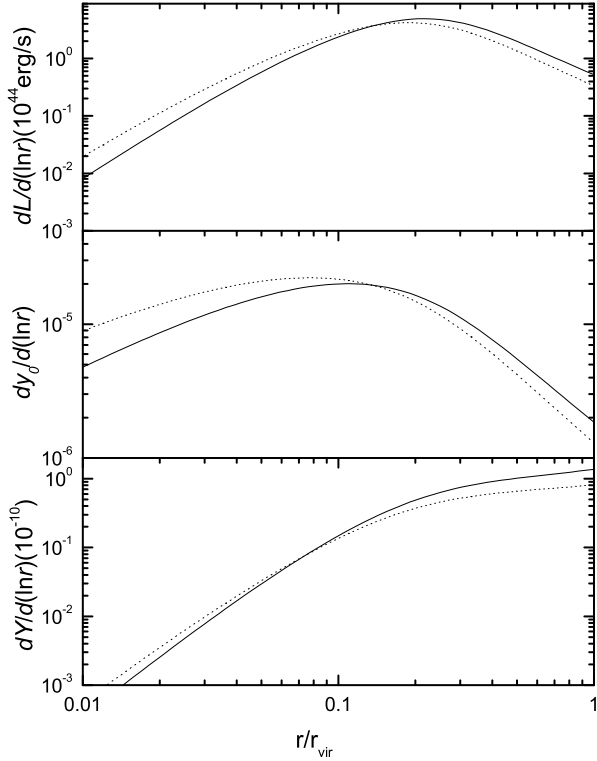


FIG. 9.— The contributions to X-ray luminosity (L , upper panel), central SZ decrement (y_0 , central panel), and the integrated SZ decrement (Y_{vir} , lower panel) from logarithmic radial bins, for both the NFW case (solid curves) and Moore et al. case (dotted curves). The profiles are shown for two clusters at $z = 0.2$ with the same temperature $T = 4.93 \text{ keV}$, predicted with $K_0 = 0$. The figure demonstrates that y_0 is more sensitive to the central regions, and is increased by steepening the DM profile though the cluster actually has a smaller M_{vir} with this profile. (See discussion in the text.)

is increased. To clarify these changes, we examined two clusters with the same temperature of $T \sim 5 \text{ keV}$ at $z = 0.2$ (predicted by setting $K_0 = 0$; we find this requires the cluster to have a mass of $M_{\text{vir}} = 9.3 \times 10^{14} M_\odot$ for the NFW case, and $M_{\text{vir}} = 7.3 \times 10^{14} M_\odot$ for the Moore et al. case). Since M_{vir} for the Moore et al. case is smaller, it is understandable that L and Y_{2500} also get smaller (from $L = 8.02 \times 10^{44} \text{ erg s}^{-1}$ to $L = 7.25 \times 10^{44} \text{ erg s}^{-1}$, and from $Y_{2500} = 5.25 \times 10^{-11}$ to $Y_{2500} = 4.65 \times 10^{-11}$). However, y_0 must be more sensitive to this steeper dark matter profile than the other two observables to finally get an increase (from $y_0 = 5.84 \times 10^{-5}$ to $y_0 = 7.18 \times 10^{-5}$). In Figure 9, we explicitly show the contributions to L , y_0 and Y_{vir} (similar to Y_{2500} , except the integration is done within the projected radius of r_{vir})⁶ from logarithmic radial bins for both the NFW case (solid curves) and Moore et al. case (dotted curves). This figure clearly shows that y_0 , L and Y are dominated by increasingly larger logarithmic radius bins. This behavior can be explained by the fact that the X-ray luminosity and the integrated SZ decrement are integrations over volume ($\propto r^3$), whereas the central SZ decrement is integration over the line of

⁶ We show Y_{vir} instead of Y_{2500} in order to remove the additional geometrical weighting of different radial bins. For reference, Y_{vir} decreases from 1.8×10^{-10} in the NFW case to 1.2×10^{-10} in the Moore et al. case.

sight ($\propto r$).

6.9. Comparison with Younger et al. (2006)

With our best-fit preheating model, adjusted to satisfy the X-ray scaling relations, and with the *WMAP* 3-year cosmology, we found that the cumulative number counts of the X-ray clusters were *underpredicted*. This is different from the conclusions in earlier work (Younger et al. 2006), which found an overprediction in a similar model (Ostriker, Bode & Babul 2005 also found an overprediction, using a higher σ_8 and a more elaborate cluster structure model). By comparing our prediction (without intrinsic scatter) with that of Younger et al. (2006), we find that the discrepancy can be attributed to four differences between our calculation and theirs. First, we use a larger value of the entropy floor in the redshift range where the clusters dominate the number counts, compared with the constant entropy floor of $194 h^{-1/3} \text{ keV cm}^2$ adopted by Younger et al. (2006). Second, we use the *WMAP* 3-year cosmological model with $\sigma_8 = 0.76$ instead of the *WMAP* 1-year cosmological model with $\sigma_8 = 0.7$. Third, in our preheating model, we use the fitting formula for the baseline entropy profile from hydrodynamic simulations, which is higher in the central regions than that adopted by Younger et al. (2006), and fourth, we also include 20% non-thermal pressure support. All of these differences (except for our larger σ_8) lead to reductions in the number density, and the amount of reduction is larger than the increase caused by σ_8 , leading to a net decrease in the predicted counts.

6.10. Expected Entropy Evolution

Since we find evidence for a significant increase in the entropy floor from the $z \sim 0.8$ to the $z \sim 0.05$ cluster sample, it is interesting to ask whether such an evolution is indeed expected if energy is continuously being injected into the intra-cluster gas. It is possible to estimate the entropy history of the IGM from the known global evolution of AGN and star formation rate. For example, Valageas & Silk (1999) find that the mean entropy level of the IGM is increasing with time in both scenarios. In this case, clusters that form at earlier times will indeed contain gas with a lower entropy floor. Assuming the resulting entropy floor can be represented by the background entropy at the formation redshift, we find the entropy floor for clusters at $z = 0.8$ evolves to $z = 0.05$ by an increase of a factor of ~ 2 , according to the calculation of Valageas & Silk (1999) for the AGN heating scenario (see their Figure 2; in the stellar heating case, the evolution is much steeper, but it is unclear whether stars can provide the necessary amount of heat). This increase is comparable to our findings: $\sim 70\%$ when we assume no intrinsic scatter, and $\sim 60\%$ when we include an intrinsic scatter. Of course, this comparison is based on a simple assumption, and the heating sources in (proto)clusters may be also different from the global average population. We leave a more serious comparison to future work.

7. CONCLUSIONS

There is ample evidence that non-gravitational processes, such as feedback from stars and BHs in galaxies, have injected excess entropy into the intracluster gas, and

therefore have modified its density profiles. While in the simplest scenario, the excess entropy is injected at high redshift, well before clusters actually form, and results in a universal entropy floor in galaxy clusters. A more realistic expectation is that the amount of excess entropy evolves with cosmic epoch, tracking on-going star and BH-formation.

Here we studied a simple model of this preheating scenario, and found that it can simultaneously explain both global X-ray scaling relations and number counts of galaxy clusters. The level of entropy required between $z = 0 - 1$ is $\sim 200 - 300 \text{ keV cm}^2$, corresponding to $\approx 0.6 - 0.9[(1 + \delta)/100]^{2/3}[(1 + z)/2]^2 \text{ keV}$ per particle if the energy is deposited in gas at overdensity δ at redshift z . This overall level of enrichment is in agreement with previous studies. Here we find, additionally, evidence that the entropy floor evolves with redshift, increasing by about $\sim 60\%$ from $z = 0.8$ to $z = 0.05$. This fractional increase is in rough agreement with the evolution expected if the heating rate follows the global evolution of the AGN. The normalization $\sigma_8 = 0.8$ preferred when X-ray cluster number counts are fit with our model is somewhat higher than the best-fit value from the three-year *WMAP* data. For a flux-limited cluster catalog, we also find that including an intrinsic scatter in log-luminosity at both fixed temperature and at fixed mass does not have a big effect on the results.

The models presented in this paper should be improved in future work, refined to fit detailed cluster profiles, in addition to the evolution of global observables, and allowing a cluster-to-cluster variation of the level of heating, with possible systematic dependence on cluster mass, in addition to redshift. It will soon be possible to confront this type of more detailed modeling with forthcoming SZ observations. We expect this comparison to securely establish whether the level of entropy is indeed increasing with cosmic epoch, and to place further interesting constraints on both cluster structure models and cosmology.

We thank Greg Bryan, Gilbert Holder, Amber Miller, Tony Mroczkowski, Josh Younger and Caleb Scharf for many useful discussions, and Greg Bryan, Stefano Ettori, Amber Miller, Josh Younger and Paolo Tozzi for helpful comments on the draft of this manuscript. We also thank Alexey Vikhlinin for providing the X-ray counts (Figure 3) and Massimiliano Bonamente and Marshall Joy for providing the SZ data (Figure 8) in electronic form, with helpful commentary. This work was supported in part by the NSF grant AST-05-07161, by the Initiatives in Science and Engineering (ISE) program at Columbia University, and by the the Polányi Program of the Hungarian National Office for Research and Technology (NKTH).

REFERENCES

- Arnaud, M. & Evrard, A. E., 1999, *MNRAS*, 305, 631
 Babul, A., Balogh, M. L., Lewis, G. F., & Poole, G. B., 2002, *MNRAS*, 330, 329
 Bahcall, N. A. & Fan, X., 1998, *ApJ*, 504, 1
 Bialek, J. J., Evrard, A. E., & Mohr, J. J. 2001, *ApJ*, 555, 597
 Blake, C. & Glazebrook, K., 2003, *ApJ*, 594, 665
 Böhringer, H. et al., 2004, *A&A*, 425, 367
 Bonamente, M. et al., 2006, *ApJ*, 647, 25
 Bonamente, M. et al., 2007, *arXiv:0708.0815*
 Bond, J. R., Cole, S., Efstathiou, G., & Kaiser, N. 1991, *ApJ*, 379, 440
 Bryan, G. L., & Norman, M. L. 1998, *ApJ*, 495, 80
 Cavaliere, A., Lapi, A., & Rephaeli, Y. 2005, *ApJ*, 634, 784
 Cavaliere, A., Menci, N., & Tozzi, P., 1997, *ApJ*, 484, L21
 Eke, V., Cole, S., & Frenk, C. S. 1996, *MNRAS*, 282, 263
 Ettori, S., Tozzi, P., Borgani, S., & Rosati, P. 2004, *A&A*, 417, 13
 Evrard, A. E. 1989, *ApJ*, 341, L71
 Evrard, A. E. & Henry, J. P., 1991, *ApJ*, 383, 95
 Evrard, A. E., Metzler, C. & Navarro, J. F. 1996, *ApJ*, 469, 494
 Faltenbacher, A., Kravtsov, A. V., Nagai, D., & Gottlober, S. 2005, *MNRAS*, 358, 139
 Haiman, Z., Mohr, J. J., & Holder, G. P. 2001, *ApJ*, 553, 545
 Henry, J. P. & Arnaud, K. A., 1991, *ApJ*, 372, 410
 Hu, W. & Haiman, Z., 2003, *Phys. Rev. D*, 68, 063004
 Jenkins, A., Frenk, C. S., White, S. D. M., Colberg, J. M., Cole, S., Evrard, A. E., Couchman, H. M. P. & Yoshida, N., 2001, *MNRAS*, 321, 372
 Kaiser, N., 1986, *MNRAS*, 222, 323
 Kaiser, N., 1991, *ApJ*, 383, 104
 Klypin, A., Kravtsov, A. V., Bullock, J. S., & Primack, J. R. 2001, *ApJ*, 554, 903
 Kuhlen, M., Strigari, L., Zetnet, A., Bullock, J. & Primack, J., 2005, *MNRAS*, 357, 387
 LaRoque, S. J. et al., 2006, *ApJ*, 652, 917
 Lesgourgues, J., Viel, M., Haehnelt, M. G. & Massey, R., 2007, *arXiv:0705.0533*
 Levine, E. S., Schultz, A. E., & White, M. 2002, *ApJ*, 577, 569
 Lima, M. & Hu, W., 2005, *Phys. Rev. D*, 72, 043006
 Lin, W. P. et al., 2006, *ApJ*, 651, 636
 Linder, E. V., 2003, *Phys. Rev. D*, 68, 083504
 Lloyd-Davies, E. J., Ponman, T. J., & Cannon, D. B., 2000, *MNRAS*, 315, 689
 Majumdar, S., & Mohr, J. J. 2004, *ApJ*, 613, 41
 Mantz, A., Allen, S. W., Ebeling, H. & Rapetti, D., 2007, *arXiv:0709.4294*
 Markevich, M. 1998, *ApJ*, 504, 27
 Maughan, B. J., Jones, L. R., Ebeling, H. & Scharf, C., 2006, *MNRAS*, 365, 509
 Mazzotta, P., Rasia, E., Moscardini, L. & Tormen, G., 2004, *MNRAS*, 354, 10
 McCarthy, I. G., Babul, A., Holder, G. P., & Balogh, M. L., 2003, 591, 526
 Miniati, F. 2005, in *Modeling the Intergalactic and Intracluster Media*, ed. V. Antonuccio-Delogu, in press(astro-ph/0401478)
 Moore, B., Governato, F., Quinn, T., Stadel, J., & Lake, G. 1998, *ApJ*, 499, L5
 Mroczkowski, T., et al. 2007, in preparation
 Muchovej, S. et al., 2007, *ApJ*, 663, 708
 Navarro, J. F., Frenk, C. S. & White, S. D. M., 1997, *ApJ*, 490, 493
 Nord, B., Stanek, R., Rasia, E. & Evrard, A. E., 2007, *arXiv:0706.2189*
 Norman, M. L., & Bryan, G. L., 1999, in *The Radio Galaxy Messier 87*, ed. H.-J. Roeser & K. Meisenheimer (New York: Springer), 106
 Ostriker, J. P., Bode, P., & Babul, A. 2005, *ApJ*, 634, 964
 Ponman, T. J., Cannon, D. B., & Navarro, J. F. 1999, *Nature*, 397, 135
 Ponman, T. J., Sanderson, A. J. R., & Finoguenov, A., 2003, *MNRAS*, 343, 331
 Pratt, G. W. & Arnaud, M., 2005, *A&A*, 429, 791
 Pratt, G. W., Arnaud, M., & Pointecouteau, E., 2006, *A&A*, 446, 429
 Press, W. H., & Schechter P. 1974, *ApJ*, 187, 425
 Raymond, J. C. & Smith, B. W., 1977, *ApJS*, 35, 419
 Reese, E. D. et al., 2002, *ApJ*, 581, 53
 Refregier, A., Valtchanov, I., & Pierre, M., 2002, *A&A*, 390, 1
 Reiprich, T. & Böhringer, H., 2002, *ApJ*, 567, 716
 Schuecker, P. et al., 2001, *A&A*, 368, 86
 Schuecker, P., Böhringer, H., Collins, C. A. & Guzzo, L., 2003, *A&A*, 398, 867
 Schuecker, P., Finoguenov, A., Miniati, F., Böhringer, H., & Briel, U. G. 2004, *A&A*, 426, 387
 Seo, H.-J. & Eisenstein, D. J., 2003, *ApJ*, 598, 720

- Sheth, R. K., & Torman, G. 1999, MNRAS, 308, 119
- Spergel, D. N. et al., 2007, ApJS, 170, 377
- Stanek, R., Evrard, A. E., Böhringer, H., Schuecker, P. & Nord, B. 2006, ApJ, 648, 956
- Tozzi, P. & Norman, C., 2001, ApJ, 546, 63
- Valageas, P., & Silk, J., 1999, A&A, 350, 725
- Viana, P. P. & Liddle, A. R., 1999, MNRAS, 303, 535
- Vikhlinin, A., McNamara, B. R., Forman, W., Jones, C., Quintana, H. & Hornstrup, A., 1998, ApJ, 502, 558 A.
- Voit, M. G., Balogh, M. L., Bower, R. G., Lacey, C. G., & Bryan, G. L., 2003, ApJ, 593, 272
- Voit, M. G., Bryan, G. L., Balogh, M. L. & Bower, R. G., 2002, ApJ, 576, 601
- Voit, M. G., Kay, S. T., & Bryan, G. L., 2005, MNRAS, 364, 909
- Wang, S., Khoury, J., Haiman, Z., May, M. 2004, Phys. Rev. D., 70, 7013008
- Well, J. & Battye, R. A., 2003, New Astronomy Reviews, 47, 775
- Weller, J., Battye, R. A., Kneissl, R., 2002, Phys. Rev. Lett., 88, 1301
- White, S. D. M., Efstathiou, G., & Frenk, C. S. 1993, MNRAS, 262, 1023
- Younger, J. D., Bryan, G. L., 2007, arXiv:0705.3465 [YB07]
- Younger, J. D., Haiman Z., Bryan, G. L. & Wang S., 2006, ApJ, 653, 27